

Femtosecond Electronic and Hydrogen Structural Dynamics in Ammonia Imaged with Ultrafast Electron Diffraction

Elio G. Champenois,¹ Nanna H. List^{2,*}, Matthew Ware,¹ Mathew Britton,^{1,3} Philip H. Bucksbaum^{1,3}, Xinxin Cheng⁴, Martin Centurion⁵, James P. Cryan¹, Ruaridh Forbes⁴, Ian Gabalski,^{1,6} Kareem Hegazy^{1,3}, Matthias C. Hoffmann,⁴ Andrew J. Howard,^{1,6} Fuhao Ji,⁴ Ming-Fu Lin⁴, J. Pedro F. Nunes⁵, Xiaozhe Shen,⁴ Jie Yang,^{4,7} Xijie Wang⁴, Todd J. Martinez^{1,8} and Thomas J. A. Wolf^{1,†}

¹Stanford PULSE Institute, SLAC National Accelerator Laboratory, Menlo Park, California 94025, USA

²Department of Chemistry, KTH Royal Institute of Technology, SE-10044 Stockholm, Sweden

³Department of Physics, Stanford University, Stanford, California 94305, USA


⁴SLAC National Accelerator Laboratory, Menlo Park, California 94025, USA

⁵Department of Physics and Astronomy, University of Nebraska Lincoln, Lincoln, Nebraska 68588, USA

⁶Department of Applied Physics, Stanford University, Stanford, California 94305, USA

⁷Department of Chemistry, Tsinghua University, Beijing 100084, China

⁸Department of Chemistry, Stanford University, Stanford, California 94305, USA

 (Received 8 March 2023; revised 6 July 2023; accepted 12 August 2023; published 5 October 2023)

Directly imaging structural dynamics involving hydrogen atoms by ultrafast diffraction methods is complicated by their low scattering cross sections. Here we demonstrate that megaelectronvolt ultrafast electron diffraction is sufficiently sensitive to follow hydrogen dynamics in isolated molecules. In a study of the photodissociation of gas phase ammonia, we simultaneously observe signatures of the nuclear and corresponding electronic structure changes resulting from the dissociation dynamics in the time-dependent diffraction. Both assignments are confirmed by *ab initio* simulations of the photochemical dynamics and the resulting diffraction observable. While the temporal resolution of the experiment is insufficient to resolve the dissociation in time, our results represent an important step towards the observation of proton dynamics in real space and time.

DOI: [10.1103/PhysRevLett.131.143001](https://doi.org/10.1103/PhysRevLett.131.143001)

Thermal and photochemical hydrogen and proton transfer reactions are among the most ubiquitous in chemistry and biology [1–3]. Directly following photochemical hydrogen and proton dynamics with time-resolved experimental methods is complicated by their fast time scales down to the few femtosecond regime. Moreover, it requires experimental methods with direct and specific sensitivity to the structural dynamics of hydrogens. Such methods, e.g., Coulomb explosion imaging (CEI), are in principle available [4–6]. The sensitivity of CEI to hydrogens has been already established for comparably complex static structures [7]. Time-resolved CEI studies of hydrogen reaction dynamics with relevance to atmospheric chemistry have been recently demonstrated [8]. However, the direct inversion of the experimentally obtained fragment momenta into molecular geometries is nontrivial for more complex structures [7,9]. Moreover, it is well established that the high optical field strengths required for multiply ionizing the molecule in CEI can themselves induce dynamics [10]. Other methods such as laser-induced electron diffraction [11–14] are able to image hydrogen motion, but have so far only been demonstrated for the observation of dynamics in photoionized, field-dressed states. Therefore, they are less suitable to investigate

hydrogen structural evolution in field-free valence excited states with broad relevance to photochemistry [15,16].

As an alternative, direct sensitivity to the motion of the nuclei can be achieved with novel time-resolved imaging methods, such as ultrafast x-ray [17–19] and electron diffraction [20–24]. In comparison to strong-field-enabled methods like CEI, time-resolved diffraction probes molecular structure through a “gentle,” i.e., elastic interaction.

Because of the exclusive interaction with the electron density of a molecule [25], the sensitivity of x-ray scattering to hydrogens and hydrogen motion is extremely limited. In contrast, electrons scatter off the Coulomb potential of a molecule, which contains contributions from both electrons and nuclei [26]. Therefore, the relative cross section of hydrogen with respect to carbon is more than an order of magnitude higher for electron compared to x-ray diffraction [27]. The observation of hydrogen motion has recently been demonstrated in bulk water using megaelectronvolt ultrafast electron diffraction (MeV UED) [24,28,29]. Here, we demonstrate that MeV UED can resolve the femtosecond excited-state hydrogen dynamics in dilute gas phase ammonia, photoexcited at ~ 200 nm.

The photodissociation of ammonia is a benchmark case for multichannel nonadiabatic photochemical dynamics

and, therefore, has been the subject of many previous experimental steady-state [30–35] and time-resolved studies [36–38], as well as theoretical investigations [39,40]. Ammonia (C_{3v} symmetry) exhibits a double minimum in its electronic ground state connected by an umbrella-type inversion motion [see potential energy surfaces, PESs, in Fig. 1(a)]. Photoexcitation around 200 nm populates the 2^1A state, which is dominated by a single-electron excitation from the nitrogen lone pair (n) orbital to a $3s$ Rydberg orbital [see visualizations in Fig. 1(a)] and, therefore, exhibits Rydberg character. The 2^1A state has a minimum at a planar geometry of D_{3h} symmetry. The large geometric difference between the ground state and 2^1A state results in a strong vibrational progression in its absorption spectrum [see Fig. 1(b)]. H_2N-H dissociation is impeded by a barrier, which can be crossed (potentially aided by tunneling) from all but the lowest two out-of-plane bending vibrational states leading to < 100 fs lifetimes in the D_{3h} minimum. Isotopic substitution with deuterium significantly increases the lifetimes in the D_{3h} minimum for a number of out-of-plane vibrational levels [30], making it easier to resolve the dynamics in time. Hence, we employ fully deuterated ammonia and excite the fourth excited state vibrational level at 202.5 nm [see Fig. 1(b)]. Deuteration only affects the timescales here, and is not expected to have any effect on the diffraction signal intensity. Thus, our findings are fully applicable to proton dynamics in general.

The dissociation barrier results from the presence of an avoided crossing between the excited Rydberg state and a higher-lying $n\sigma^*$ state with D_2N-D antibonding character [44]. Thus, the excited state gradually changes its electronic character from $n3s$ to $n\sigma^*$ along the D_2N-D dissociation coordinate. After passing the dissociation barrier, the wave packet proceeds along the D_2N-D coordinate towards adiabatic and nonadiabatic photodissociation channels, yielding $ND_2(\tilde{X}) + D$ and $ND_2(\tilde{A}) + D$ (see Fig. 1).

The sensitivity of electron scattering to the electronic structure of molecules has long been established and benchmarked, among other molecules, with the help of ammonia [45–47]. Elastic scattering processes are sensitive to the electron density in a molecule. In contrast, inelastic scattering is sensitive to electron correlation [48]. We have recently demonstrated that inelastic scattering can be employed to follow electronic structure changes during photochemical dynamics [21]. Such changes in electron correlation can originate from population transfer between excited states of different electronic character through conical intersections [21] or due to more gradual excited-state character changes like the change $n3s$ to $n\sigma^*$ when crossing the excited-state barrier of ammonia.

The strongest contributions from inelastic scattering appear at momentum transfer values $< 2 \text{ \AA}^{-1}$ whereas difference diffraction signatures of nuclear geometry changes can typically be measured up to 10 \AA^{-1} [22]. Thus, complementary information from electronic- and nuclear-structure

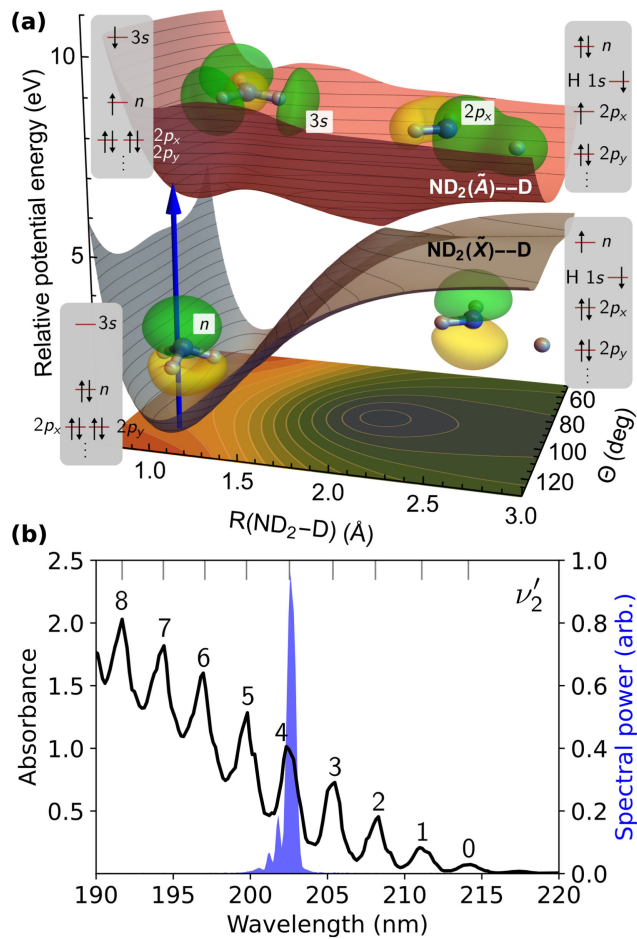


FIG. 1. (a) S_0 and S_1 PESs (obtained from Refs. [40,41]) along the umbrella (Θ) and ND_2-D dissociation coordinates. Photoexcitation (blue arrow) to the predissociative 2^1A state activates the umbrella mode and promotes adiabatic or non-adiabatic ND_2-D dissociation. The contour plot shows the S_1/S_0 energy gap, indicating a smaller gap (blue) along the ND_2-D coordinate. Key orbitals involved in the process are shown as insets and correspond to state-averaged natural orbitals (isovalue = 0.36 a.u.). The Rydberg orbital correlates with a σ^* orbital in the distorted ND_2-D and eventually becomes the $1s$ H orbital upon dissociation. Additionally, the dominant electron configurations (nonspin adapted) of the states in the Franck-Condon region and in the dissociation limit are shown. (b) Experimental absorption spectrum of ND_3 (black line) showing strong vibrational progression in the umbrella mode (ν_2'). The peaks of the progression are labeled with respect to the corresponding vibrational level. The small peak at 217 nm results from a hot band of ND_3 [42,43]. The spectrum of the UV pump laser centered around $\nu_2' = 4$ of the umbrella mode is shown in blue.

changes can be detected in a well-separable fashion in the experimental diffraction patterns. In the present study, we observe, in addition to signatures of the structural N–D dissociation, clear signatures of the electronic excitation and electronic character change from $n3s$ to $n\sigma^*$.

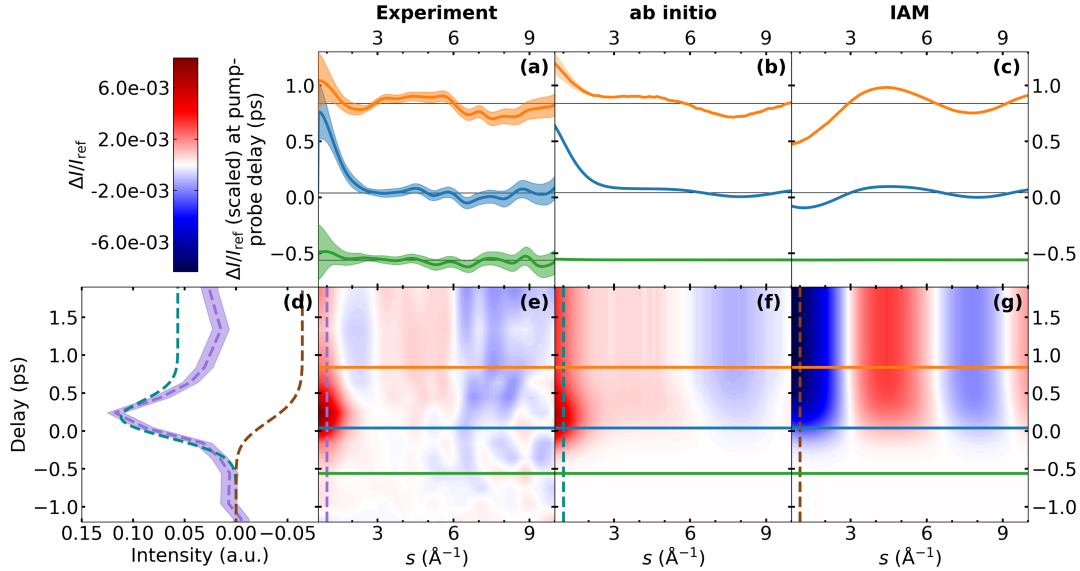


FIG. 2. Comparison of experimental and simulated signatures. (a)–(c) show $\Delta I/I_{\text{ref}}$ signals at different delays from (a) the experiment, (b) *ab initio* scattering calculations based on AIMS simulations, and (c) the same AIMS simulations, but using the independent atom model (IAM) to compute the diffraction signal. The delays for the temporal lineouts in (a)–(c) are marked as color-coded horizontal lines in the corresponding false-color plots of the time-dependent signals from the experiment and the two different simulation approaches in (e)–(g). Additionally, the time dependence of the integrated low- s regions of the three false-color plots is shown in plot (d) where the upper- s integration limits are marked by vertical color-coded dashed lines in plots (e)–(g).

The experiment was performed at the MeV UED facility at SLAC National Accelerator Laboratory [49]. Figure S1 shows a schematic of the experimental setup. A 202.5 nm pump pulse was spatially and temporally overlapped with an electron pulse of 4.2 MeV kinetic energy in a pulsed jet of ND₃. Diffracted electrons were detected with a combination of a phosphor screen and a camera. The simulations were performed using *ab initio* multiple spawning [50] (AIMS) in combination with *ab initio* elastic and inelastic electron scattering simulations [21]. A detailed description of both the experimental and theoretical methods can be found in Sec. S1 of the Supplemental Material [51].

Our AIMS simulations are based on the PESs and nonadiabatic couplings reported by Yarkony *et al.* [40,41] and provide a picture consistent with previous numerically exact quantum dynamics [40]. In particular, following photoexcitation and progress along the D₂N-D dissociation coordinate (Sec. S2 and Fig. S4), the majority of the population undergoes nonadiabatic photodissociation ($\sim 66\%$) with a smaller portion ($\sim 24\%$) proceeding along the adiabatic channel (Fig. S5). A small fraction ($< 10\%$) remains trapped (after 0.84 ps) on the excited state by the predissociation barrier and hence retains Rydberg character (Fig. S6).

In Fig. 2(e), we present the results of our MeV UED experiment as a false-color plot in the form of the difference between the time-dependent diffraction and the static diffraction of ND₃ normalized by the static diffraction [$\Delta I/I_{\text{ref}}(s, t)$, where s is the momentum transfer in \AA^{-1}]. Additionally, Fig. 2(a) shows $\Delta I/I_{\text{ref}}(s)$ at the three

different delay times ($t = -0.56$ ps, 0.04 ps, and 0.84 ps), which are marked by the color-coded horizontal lines in Fig. 2(e). These delay times are chosen to include one delay clearly before time zero as a reference for the noise level of the experimental signals, the closest experimental delay to time zero, and one delay where the dissociation reaction is expected to be finished. The s -integrated $\Delta I/I_{\text{ref}}(0.67 \text{\AA}^{-1} < s < 1 \text{\AA}^{-1}, t)$ [dashed purple vertical line in Fig. 2(e)] is shown in Fig. 2(d), purple. At time zero, a strong positive feature turns on in the $s < 2 \text{\AA}^{-1}$ regime and decays within the instrument response function (500-fs full width at half maximum, FWHM) to a weaker, delay-independent level [Fig. 2(d)]. Simultaneously, substantially weaker features appear: specifically, a broad positive signature between 3 and 6 \AA^{-1} and a broad negative signature at $s > 6 \text{\AA}^{-1}$ that stay constant over the whole remaining time delay window.

The experimental results in Fig. 2(e) are compared with the simulated scattering signals computed based on AIMS dynamics of photoexcited ND₃ (see Secs. S1 D and S2). We use two different approaches to simulate the electron diffraction observable from the simulated wave packet. First, using *ab initio* scattering where the $\Delta I/I_{\text{ref}}(s, t)$ signatures are computed by scattering off the Coulomb potential from the nuclei and the electronic wave function as evaluated in our wave packet simulations [Figs. 2(b) and 2(f)]. This scattering simulation includes both elastic and inelastic scattering contributions. Analogous to the experimental data, the time dependence of the integrated difference diffraction $0.67 \text{\AA}^{-1} < s < 1 \text{\AA}^{-1}$ is plotted in

Fig. 2(d) (dashed cyan line). Second, we also provide $\Delta I/I_{\text{ref}}(s, t)$ signatures based on the independent atom model [IAM, Figs. 2(c) and 2(g)] that neglect both inelastic scattering and changes in electron density around individual atoms due to chemical bonding or electron density redistribution (e.g., following electronic excitation). The time dependence of the integrated signal at low s values is plotted in Fig. 2(d) (dashed brown line).

To understand the time-dependent signatures in Fig. 2, we begin by considering the respective signatures at late delays [Figs. 2(a)–2(c), orange] when the photodissociation is complete [see Fig. 1(a)]. The signature from the IAM scattering simulation in Fig. 2(c) exclusively originates from changes in the nuclear geometry (interatomic distances) due to the atomic superposition approximation inherent to the IAM. Since it is a $\Delta I/I_{\text{ref}}(s, t)$ signature, it results from the difference of signatures from the atomic distances in and between the dissociation products at a delay time of 0.84 ps and signatures from the distances in the ND₃ reactant geometry. Because of the relatively large atomic form factor of nitrogen, it is dominated by the difference of N–D distance signatures from the evolving photoexcited population and from the reactant geometry (see Sec. S3 for details). Moreover, the presence of the predissociation barrier [see S_1 potential surface in Fig. 1(a)] leads to a blurring of the diffraction signatures from the photoexcited population. This effect is further increased by the limited time resolution of the experiment (modeled in the IAM simulations in Fig. 2 by convolution with a Gaussian in time, see Sec. S1 D). The signature at late delays in the IAM simulation [Fig. 2(c)] is, therefore, dominated by the loss of one N–D bond distance (see Sec. S3).

A qualitatively similar, but weaker, signal is found both in the experimental and *ab initio* scattering signatures for $s > 3 \text{ \AA}^{-1}$ [Figs. 2(a) and 2(b)]. A decomposition of the *ab initio* scattering signature into elastic and inelastic scattering contributions (Figs. 3 and S7) shows that it is exclusively due to elastic scattering. Because of the incoherent nature of inelastic scattering, we do not expect any direct signatures from changes in the molecular geometry [21]. Thus, the absence of the signature at $s > 3 \text{ \AA}^{-1}$ in the inelastic scattering supports the assignment of this signature as the loss of one N–D bond, analogous to the IAM scattering signature. The relative weakness of the signatures with respect to the IAM simulation is a direct result of the deviation of the actual electron distribution in ND₃ from a superposition of atomic densities assumed in the IAM.

Considering next the low- s ($s < 3 \text{ \AA}^{-1}$) region at late delays (orange plots), the *ab initio* scattering and experimental signals deviate qualitatively from the IAM. Both show a strong positive signature for $s < 1 \text{ \AA}^{-1}$ whereas the IAM simulations exhibit a negative signature. Decomposition of the *ab initio* scattering simulations (Figs. 3 and S7)

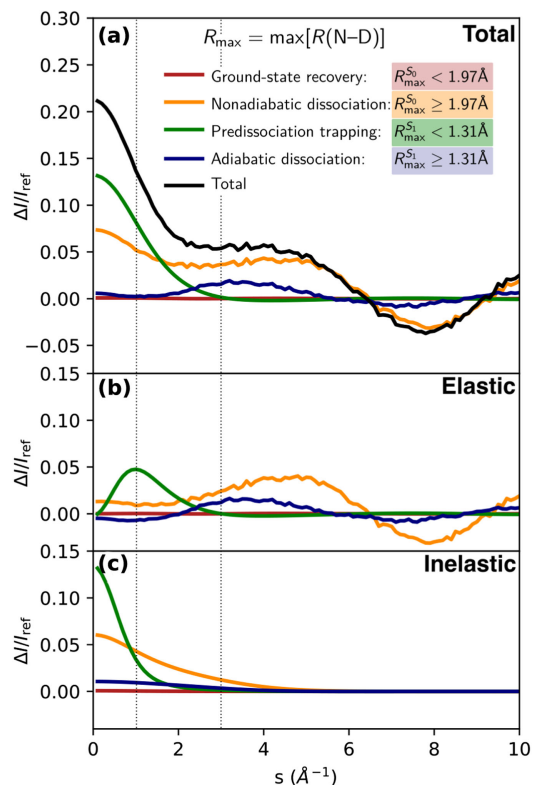


FIG. 3. Decomposition of the *ab initio* scattering signal at $t = 0.84$ ps according to the exit channel. (a) Total scattering signal, and its decomposition into (b) elastic and (c) inelastic components. The vertical dashed lines mark $s = 1$ and 3 \AA^{-1} . The distance-based cutoffs used to define the photoproducts are indicated in the figure (see also Fig. S5).

shows that its main contribution below 1 \AA^{-1} originates from the small fraction ($< 10\%$, Fig. S5) of population that is trapped behind the S_1 predissociation barrier [see Fig. 1(a)]. As shown in Fig. S6, this is mainly due to the Rydberg character of the excited state rather than geometric changes from the difference between ground-state and excited-state potentials in the Franck-Condon region.

It should be noted that both elastic and inelastic scattering contribute to the low- s signature (see Figs. 3 and S7). Both contributions can be directly connected to the Rydberg character of the excited state. First, the strength of the elastic scattering contribution originates from the significant change in electron density distribution induced by the Rydberg excitation: one electron, i.e., 10% of the overall electron density, is redistributed from a fairly localized lone pair orbital to a strongly delocalized Rydberg orbital. Second, the excitation from the electronic ground state (strongly correlated motion of the two electrons occupying the n orbital) to a $n3s$ Rydberg state (weak correlation between the remaining n electron and the $3s$ electron) can be expected to yield a significant change in the inelastic scattering signature.

Weaker contributions to the $s < 1 \text{ \AA}^{-1}$ signal arise from the large population ($\sim 66\%$) in the nonadiabatic dissociation channel, mainly from inelastic scattering contributions (see Fig. 3). The less populated adiabatic dissociation channel ($\sim 24\%$) shows negligible contributions in this region. The disagreement between experimental and *ab initio* scattering simulation between $1 < s < 2 \text{ \AA}^{-1}$ can be explained by a baseline offset in the experimental data in this region in combination with a slight overestimation of the inelastic scattering intensities in the *ab initio* simulations.

Summing up our theoretical analysis at long time delays, we can distinguish two regions in the $\Delta I/I_{\text{ref}}(s, t)$ signal: (i) the $< 1 \text{ \AA}^{-1}$ region which is almost exclusively sensitive to the electronic character of the excited electronic state, and (ii) the $> 3 \text{ \AA}^{-1}$ region which has exclusive sensitivity to nuclear structural changes, i.e., the loss of an N–D bond upon photodissociation.

We can interpret the time-zero signal [blue curves in Figs. 2(a)–2(c)] along the same s regions. Experimental and *ab initio* scattering signals are dominated by a stronger signature at $s < 1 \text{ \AA}^{-1}$ than at later delay times. The region at $s > 3 \text{ \AA}^{-1}$ shows the same (albeit weaker) signatures as at later delay times. The strong signature at $s < 1 \text{ \AA}^{-1}$ is easily explained by the fact that initially all of the excited-state population is residing behind the predissociation barrier, where the electronic state exhibits Rydberg character [see Fig. 1(a)]. Accordingly, the decay of the signal at $s < 1 \text{ \AA}^{-1}$ after time zero is related to the depopulation of the quasibound Franck-Condon region across or through the predissociation barrier due to the associated change in electronic character (see also Fig. S6). Since the IAM is insensitive to the electronic state, this feature is entirely missing in the IAM scattering signal. The weak dissociation signatures at $s > 3 \text{ \AA}^{-1}$ are the result of a temporal smearing of the onset of the dissociation signatures due to the limited temporal resolution (see Fig. S7 for the raw, i.e., without temporal convolution, theoretical difference scattering signals).

In conclusion, we observed signatures from both deuterium structural dynamics and electronic structure changes during the photodissociation of ND_3 in well-separated momentum transfer ranges of ultrafast electron diffraction. The ability to follow the complementary information of the nuclear and electronic structure evolution in well-separable observables is so far unmatched by other methods and marks a powerful demonstration of the ability of MeV UED to follow nonadiabatic proton and hydrogen photochemistry. Our results lack, so far, in temporal resolution (500 fs FWHM), a crucial parameter for the investigation of photochemical reaction dynamics involving hydrogens and protons. However, structural dynamics of more strongly scattering second row elements can already be investigated at the existing MeV UED facility using lower

electron pulse charges, which result in a threefold improved time resolution (150 fs FWHM) [22]. The signal levels required for the observation of proton dynamics at this higher temporal resolution can be achieved, e.g., by an increase of the repetition rate to the MHz regime as already demonstrated for electron injector guns for next-generation x-ray-free electron lasers.

We thank Dr. Xiaolei Zhu for helpful discussions. This work was supported by the AMOS program within the U.S. Department of Energy (DOE), Office of Science, Basic Energy Sciences, Chemical Sciences, Geosciences, and Biosciences Division. N. H. L. acknowledges start-up funding from the School of Engineering Sciences in Chemistry, Biotechnology and Health (CBH), KTH Royal Institute of Technology. M. C. and J. P. F. N. acknowledge funding from the DOE Office of Basic Energy Sciences, Chemical Sciences, Geosciences, and Biosciences Division, AMOS program, under Award No. DE-SC0014170. The experiments were performed at the MeV UED facility. MeV UED is operated as part of the Linac Coherent Light Source at the SLAC National Accelerator Laboratory, supported in part by the U.S. Department of Energy (DOE) Office of Science, Office of Basic Energy Sciences, SUF Division Accelerator and Detector R&D program, the LCLS Facility, and SLAC under Contracts No. DE-AC02-05CH11231 and No. DE-AC02-76SF00515. I. G. was supported by an NDSEG Fellowship.

*nalist@kth.se

†thomas.wolf@stanford.edu

- [1] S. Y. Reece and D. G. Nocera, Proton-coupled electron transfer in biology: Results from synergistic studies in natural and model systems, *Annu. Rev. Biochem.* **78**, 673 (2009).
- [2] S. Hammes-Schiffer and A. A. Stuchebrukhov, Theory of coupled electron and proton transfer reactions, *Chem. Rev.* **110**, 6939 (2010).
- [3] P. Goyal and S. Hammes-Schiffer, Tuning the ultrafast dynamics of photoinduced proton-coupled electron transfer in energy conversion processes, *ACS Energy Lett.* **2**, 512 (2017).
- [4] F. Légaré, K. F. Lee, I. V. Litvinyuk, P. W. Dooley, A. D. Bandrauk, D. M. Villeneuve, and P. B. Corkum, Imaging the time-dependent structure of a molecule as it undergoes dynamics, *Phys. Rev. A* **72**, 052717 (2005).
- [5] H. Stapelfeldt, E. Constant, H. Sakai, and P. B. Corkum, Time-resolved Coulomb explosion imaging: A method to measure structure and dynamics of molecular nuclear wave packets, *Phys. Rev. A* **58**, 426 (1998).
- [6] M. Pitzer, M. Kunitski, A. S. Johnson, T. Jahnke, H. Sann, F. Sturm, L. P. H. Schmidt, H. Schmidt-Bocking, R. Dörner, J. Stohner, J. Kiedrowski, M. Reggelin, S. Marquardt, A. Schiesser, R. Berger, and M. S. Schoffler, Direct determination of absolute molecular stereochemistry in gas phase by Coulomb explosion imaging, *Science* **341**, 1096 (2013).

- [7] R. Boll *et al.*, X-ray multiphoton-induced Coulomb explosion images complex single molecules, *Nat. Phys.* **18**, 1 (2022).
- [8] T. Endo, S. P. Neville, V. Wanie, S. Beaulieu, C. Qu, J. Deschamps, P. Lassonde, B. E. Schmidt, H. Fujise, M. Fushitani, A. Hishikawa, P. L. Houston, J. M. Bowman, M. S. Schuurman, F. c. Légaré, and H. Ibrahim, Capturing roaming molecular fragments in real time, *Science* **370**, 1072 (2020).
- [9] X. Li *et al.*, Coulomb explosion imaging of small polyatomic molecules with ultrashort x-ray pulses, *Phys. Rev. Res.* **4**, 013029 (2022).
- [10] M. Kübel, R. Siemering, C. Burger, N. G. Kling, H. Li, A. S. Alnaser, B. Bergues, S. Zhrebtsov, A. M. Azzeer, I. Ben-Itzhak, R. Moshhammer, R. de Vivie-Riedle, and M. F. Kling, Steering Proton Migration in Hydrocarbons Using Intense Few-Cycle Laser Fields, *Phys. Rev. Lett.* **116**, 193001 (2016).
- [11] M. G. Pullen, B. Wolter, A.-T. Le, M. Baudisch, M. Hemmer, A. Senftleben, C. D. Schröter, J. Ullrich, R. Moshhammer, C. D. Lin, and J. Biegert, Imaging an aligned polyatomic molecule with laser-induced electron diffraction, *Nat. Commun.* **6**, 7262 (2015).
- [12] B. Wolter, M. G. Pullen, A.-T. Le, M. Baudisch, K. Doblhoff-Dier, A. Senftleben, M. Hemmer, C. D. Schröter, J. Ullrich, T. Pfeifer, R. Moshhammer, S. Gräfe, O. Vendrell, C. D. Lin, and J. Biegert, Ultrafast electron diffraction imaging of bond breaking in di-ionized acetylene, *Science* **354**, 308 (2016).
- [13] A. Sanchez, K. Amini, S.-J. Wang, T. Steinle, B. Belsa, J. Danek, A. T. Le, X. Liu, R. Moshhammer, T. Pfeifer, M. Richter, J. Ullrich, S. Gräfe, C. D. Lin, and J. Biegert, Molecular structure retrieval directly from laboratory-frame photoelectron spectra in laser-induced electron diffraction, *Nat. Commun.* **12**, 1520 (2021).
- [14] B. Belsa, K. Amini, X. Liu, A. Sanchez, T. Steinle, J. Steinmetzer, A. T. Le, R. Moshhammer, T. Pfeifer, J. Ullrich, R. Moszynski, C. D. Lin, S. Gräfe, and J. Biegert, Laser-induced electron diffraction of the ultrafast umbrella motion in ammonia, *Struct. Dyn.* **8**, 014301 (2021).
- [15] V. Hanus, S. Kangaparambil, S. Larimian, M. Dorner-Kirchner, X. Xie, M. S. Schöffler, G. G. Paulus, A. Baltuška, A. Staudte, and M. Kitzler-Zeiler, Subfemtosecond Tracing of Molecular Dynamics During Strong-Field Interaction, *Phys. Rev. Lett.* **123**, 263201 (2019).
- [16] V. Hanus, S. Kangaparambil, S. Larimian, M. Dorner-Kirchner, X. Xie, M. S. Schöffler, G. G. Paulus, A. Baltuška, A. Staudte, and M. Kitzler-Zeiler, Experimental Separation of Subcycle Ionization Bursts in Strong-Field Double Ionization of H_2 , *Phys. Rev. Lett.* **124**, 103201 (2020).
- [17] M. P. Minitti, J. M. Budarz, A. Kirrander, J. S. Robinson, D. Ratner, T. J. Lane, D. Zhu, J. M. Glowina, M. Kozina, H. T. Lemke, M. Sikorski, Y. Feng, S. Nelson, K. Saita, B. Stankus, T. Northey, J. B. Hastings, and P. M. Weber, Imaging Molecular Motion: Femtosecond X-Ray Scattering of an Electrocyclic Chemical Reaction, *Phys. Rev. Lett.* **114**, 255501 (2015).
- [18] B. Stankus, H. Yong, N. Zotev, J. M. Ruddock, D. Bellshaw, T. J. Lane, M. Liang, S. Boutet, S. Carbajo, J. S. Robinson, W. Du, N. Goff, Y. Chang, J. E. Koglin, M. P. Minitti, A. Kirrander, and P. M. Weber, Ultrafast x-ray scattering reveals vibrational coherence following rydberg excitation, *Nat. Chem.* **11**, 716 (2019).
- [19] J. M. Ruddock, H. Yong, B. Stankus, W. Du, N. Goff, Y. Chang, A. Odate, A. M. Carrascosa, D. Bellshaw, N. Zotev, M. Liang, S. Carbajo, J. Koglin, J. S. Robinson, S. Boutet, A. Kirrander, M. P. Minitti, and P. M. Weber, A deep UV trigger for ground-state ring-opening dynamics of 1,3-cyclohexadiene, *Sci. Adv.* **5**, eaax6625 (2019).
- [20] J. Yang, X. Zhu, T. J. A. Wolf, Z. Li, J. P. F. Nunes, R. Coffee, J. P. Cryan, M. Gühr, K. Hegazy, T. F. Heinz, K. Jobe, R. Li, X. Shen, T. Veccione, S. Weathersby, K. J. Wilkin, C. Yoneda, Q. Zheng, T. J. Martinez, M. Centurion, and X. Wang, Imaging CF3I conical intersection and photodissociation dynamics with ultrafast electron diffraction, *Science* **361**, 64 (2018).
- [21] J. Yang, X. Zhu, J. P. F. Nunes, J. K. Yu, R. M. Parrish, T. J. A. Wolf, M. Centurion, M. Gühr, R. Li, Y. Liu, B. Moore, M. Niebuhr, S. Park, X. Shen, S. Weathersby, T. Weinacht, T. J. Martinez, and X. Wang, Simultaneous observation of nuclear and electronic dynamics by ultrafast electron diffraction, *Science* **368**, 885 (2020).
- [22] T. J. A. Wolf *et al.*, The photochemical ring-opening of 1,3-cyclohexadiene imaged by ultrafast electron diffraction, *Nat. Chem.* **11**, 504 (2019).
- [23] E. G. Champenois, D. M. Sanchez, J. Yang, J. P. Figueira Nunes, A. Attar, M. Centurion, R. Forbes, M. Gühr, K. Hegazy, F. Ji, S. K. Saha, Y. Liu, M.-F. Lin, D. Luo, B. Moore, X. Shen, M. R. Ware, X. J. Wang, T. J. Martínez, and T. J. A. Wolf, Conformer-specific photochemistry imaged in real space and time, *Science* **374**, 178 (2021).
- [24] J. Yang *et al.*, Direct observation of ultrafast hydrogen bond strengthening in liquid water, *Nature (London)* **596**, 531 (2021).
- [25] A. Moreno Carrascosa, H. Yong, D. L. Crittenden, P. M. Weber, and A. Kirrander, *Ab Initio* calculation of total x-ray scattering from molecules, *J. Chem. Theory Comput.* **15**, 2836 (2019).
- [26] M. Centurion, T. J. Wolf, and J. Yang, Ultrafast imaging of molecules with electron diffraction, *Annu. Rev. Phys. Chem.* **73**, 21 (2022).
- [27] J. H. Hubbell, W. J. Veigle, E. A. Briggs, R. T. Brown, D. T. Cromer, and R. J. Howerton, Atomic form factors, incoherent scattering functions, and photon scattering cross sections, *J. Phys. Chem. Ref. Data* **4**, 471 (1975).
- [28] J. P. F. Nunes, K. Ledbetter, M. Lin, M. Kozina, D. P. DePonte, E. Biasin, M. Centurion, C. J. Crissman, M. Dunning, S. Guillet, K. Jobe, Y. Liu, M. Mo, X. Shen, R. Sublett, S. Weathersby, C. Yoneda, T. J. A. Wolf, J. Yang, A. A. Cordones, and X. J. Wang, Liquid-phase mega-electron-volt ultrafast electron diffraction, *Struct. Dyn.* **7**, 024301 (2020).
- [29] M.-F. Lin, N. Singh, S. Liang, M. Mo, J. P. F. Nunes, K. Ledbetter, J. Yang, M. Kozina, S. Weathersby, X. Shen, A. A. Cordones, T. J. A. Wolf, C. D. Pemmaraju, M. Ihme, and X. J. Wang, Imaging the short-lived hydroxyl-hydronium pair in ionized liquid water, *Science* **374**, 92 (2021).
- [30] V. Vaida, M. McCarthy, P. Engelking, P. Rosmus, H.-J. Werner, and P. Botschwina, The ultraviolet absorption

- spectrum of the $\tilde{A}^1A_2' \leftarrow \tilde{X}^1A_1$ transition of jet-cooled ammonia, *J. Chem. Phys.* **86**, 6669 (1987).
- [31] M. N. R. Ashfold, C. L. Bennett, and R. N. Dixon, Predissociation dynamics of \tilde{A} -state ammonia probed by two-photon excitation spectroscopy, *Chem. Phys.* **93**, 293 (1985).
- [32] M. Ashfold, S. Langford, R. Morgan, A. Orr-Ewing, C. Western, C. Scheper, and C. de Lange, Resonance enhanced multiphoton ionization (REMPI) and REMPI-photoelectron spectroscopy of ammonia, *Eur. Phys. J. D* **4**, 189 (1998).
- [33] M. L. Hause, Y. H. Yoon, and F. F. Crim, Vibrationally mediated photodissociation of ammonia: The influence of N-H stretching vibrations on passage through conical intersections, *J. Chem. Phys.* **125**, 174309 (2006).
- [34] D. H. Mordaunt, M. N. R. Ashfold, and R. N. Dixon, Photodissociation dynamics of \tilde{A} state ammonia molecules. I. State dependent μ - ν correlations in the NH₂(ND₂) products, *J. Chem. Phys.* **104**, 6460 (1996).
- [35] J. D. Rodríguez, M. G. González, L. Rubio-Lago, and L. Bañares, A velocity map imaging study of the photodissociation of the \tilde{A} state of ammonia, *Phys. Chem. Chem. Phys.* **16**, 406 (2014).
- [36] A. S. Chatterley, G. M. Roberts, and V. G. Stavros, Time-scales for adiabatic photodissociation dynamics from the \tilde{A} state of ammonia, *J. Chem. Phys.* **139**, 034318 (2013).
- [37] N. L. Evans, H. Yu, G. M. Roberts, V. G. Stavros, and S. Ullrich, Observation of ultrafast nh₃ (\tilde{A}) state relaxation dynamics using a combination of time-resolved photoelectron spectroscopy and photoproduct detection, *Phys. Chem. Chem. Phys.* **14**, 10401 (2012).
- [38] H. Yu, N. L. Evans, A. S. Chatterley, G. M. Roberts, V. G. Stavros, and S. Ullrich, Tunneling dynamics of the NH₃ (\tilde{A}) state observed by time-resolved photoelectron and H atom kinetic energy spectroscopies, *J. Phys. Chem. A* **118**, 9438 (2014).
- [39] C. Xie, X. Zhu, J. Ma, D. R. Yarkony, D. Xie, and H. Guo, Communication: On the competition between adiabatic and nonadiabatic dynamics in vibrationally mediated ammonia photodissociation in its A band, *J. Chem. Phys.* **142**, 091101 (2015).
- [40] J. Ma, X. Zhu, H. Guo, and D. R. Yarkony, First principles determination of the nh₂/nd₂(\tilde{A}/\tilde{X}) branching ratios for photodissociation of nh₃/nd₃ via full-dimensional quantum dynamics based on a new quasi-diabatic representation of coupled *ab initio* potential energy surfaces, *J. Chem. Phys.* **137**, 22A541 (2012).
- [41] X. Zhu and D. R. Yarkony, On the representation of coupled adiabatic potential energy surfaces using quasi-diabatic hamiltonians: A distributed origins expansion approach, *J. Chem. Phys.* **136**, 174110 (2012).
- [42] F. Chen, D. Judge, C. Wu, and J. Caldwell, Low and room temperature photoabsorption cross sections of nh₃ in the uv region, *Planet. Space Sci.* **47**, 261 (1998).
- [43] B.-M. Cheng, H.-C. Lu, H.-K. Chen, M. Bahou, Y.-P. Lee, A. M. Mebel, L.-C. Lee, M.-C. Liang, and Y. L. Yung, Absorption cross sections of nh₃, nh₂d, nhd₂, and nd₃ in the spectral range 140–220 nm and implications for planetary isotopic fractionation, *Astrophys. J.* **647**, 1535 (2006).
- [44] M. N. R. Ashfold, G. A. King, D. Murdock, M. G. D. Nix, T. A. A. Oliver, and A. G. Sage, $\pi\sigma^*$ excited states in molecular photochemistry, *Phys. Chem. Chem. Phys.* **12**, 1218 (2010).
- [45] A. L. Bennani, A. Duguet, and H. F. Wellenstein, Differential cross sections for 35 keV electrons elastically scattered from NH₃, *J. Phys. B* **12**, 461 (1979).
- [46] A. Duguet, A. Lahmam-Bennani, and M. Rouault, High energy elastic and inelastic electron scattering by the NH₃ molecule-binding effect, *J. Chem. Phys.* **78**, 6595 (1983).
- [47] M. Breitenstein, H. Meyer, and A. Schweig, CI calculations of electron and x-ray scattering cross sections of non-linear molecules: H₂O and NH₃, *Chem. Phys.* **112**, 199 (1987).
- [48] L. S. Bartell and R. M. Gavin, Effects of electron correlation in x-ray and electron diffraction, *J. Am. Chem. Soc.* **86**, 3493 (1964).
- [49] X. Shen, J. P. F. Nunes, J. Yang, R. K. Jobe, R. K. Li, M.-F. Lin, B. Moore, M. Niebuhr, S. P. Weathersby, T. J. A. Wolf, C. Yoneda, M. Guehr, M. Centurion, and X. J. Wang, Femtosecond gas-phase mega-electron-volt ultrafast electron diffraction, *Struct. Dyn.* **6**, 054305 (2019).
- [50] M. Ben-Nun, J. Quenneville, and T. J. Martínez, *Ab initio* multiple spawning: Photochemistry from first principles quantum molecular dynamics, *J. Phys. Chem. A* **104**, 5161 (2000).
- [51] See Supplemental Material at <http://link.aps.org/supplemental/10.1103/PhysRevLett.131.143001> for additional information and methodological details, which includes Refs. [52–59].
- [52] M. D. Hack, A. M. Wensmann, D. G. Truhlar, M. Ben-Nun, and T. J. Martínez, Comparison of full multiple spawning, trajectory surface hopping, and converged quantum mechanics for electronically nonadiabatic dynamics, *J. Chem. Phys.* **115**, 1172 (2001).
- [53] I. S. Ufimtsev and T. J. Martínez, Quantum chemistry on graphical processing units. 1. Strategies for two-electron integral evaluation, *J. Chem. Theory Comput.* **4**, 222 (2008).
- [54] I. S. Ufimtsev and T. J. Martínez, Quantum chemistry on graphical processing units. 2. direct self-consistent-field implementation, *J. Chem. Theory Comput.* **5**, 1004 (2009).
- [55] I. S. Ufimtsev and T. J. Martínez, Quantum chemistry on graphical processing units. 3. Analytical energy gradients, geometry optimization, and first principles molecular dynamics, *J. Chem. Theory Comput.* **5**, 2619 (2009).
- [56] S. Seritan, C. Bannwarth, B. S. Fales, E. G. Hohenstein, C. M. Isborn, S. I. L. Kokkila-Schumacher, X. Li, F. Liu, N. Luehr, J. W. Snyder Jr., C. Song, A. V. Titov, I. S. Ufimtsev, L.-P. Wang, and T. J. Martínez, Terachem: A graphical processing unit-accelerated electronic structure package for large-scale *ab initio* molecular dynamics, *Comput. Mol. Sci.* **11**, e1494 (2021).
- [57] C. Colliex, J. M. Cowley, S. L. Dudarev, M. Fink, J. Gjønnnes, R. Hilderbrandt, A. Howie, D. F. Lynch, L. M. Peng, G. Ren, A. W. Ross, V. H. Smith, J. C. H. Spence, J. W. Steeds, J. Wang, M. J. Whelan, and B. B. Zvyagin, Electron diffraction, in *International Tables for Crystallography Volume C: Mathematical, Physical and Chemical Tables*, International Tables for Crystallography, edited by E. Prince (Springer Netherlands, Dordrecht, 2004), pp. 259–429.

- [58] J. Biesner, L. Schnieder, J. Schmeer, G. Ahlers, X. Xie, K. H. Welge, M. N. R. Ashfold, and R. N. Dixon, State selective photodissociation dynamics of \tilde{A} state ammonia. I, *J. Chem. Phys.* **88**, 3607 (1988).
- [59] J. Biesner, L. Schnieder, G. Ahlers, X. Xie, K. H. Welge, M. N. R. Ashfold, and R. N. Dixon, State selective photodissociation dynamics of \tilde{A} state ammonia. II, *J. Chem. Phys.* **91**, 2901 (1989).